

Regularized lattice Boltzmann Multicomponent models for low Capillary and Reynolds microfluidics flows.

Andrea Montessori ^{*1}, Marco Lauricella², Michele La Rocca¹, Sauro Succi^{2,3}, Elad Stolovicki⁴, Roy Ziblat⁴, and David Weitz^{5,4}

¹Department of Engineering, University of Rome "Roma Tre," Via della Vasca Navale 79, 00141 Rome, Italy

²Istituto per le Applicazioni del Calcolo CNR, Via dei Taurini 19, 00185 Rome, Italy

³Institute for Applied Computational Science, Harvard John A. Paulson School of Engineering And Applied Sciences, Cambridge, MA 02138, United States

⁴School of Engineering and Applied Sciences, Harvard University, McKay 517 Cambridge, MA 02138, USA

⁵Department of Physics, and School of Engineering and Applied Sciences, Harvard University, Pierce 231, 29 Oxford St. Cambridge, MA 02138, USA

Monday 30th October, 2017

Abstract

We present a regularized version of the color gradient lattice Boltzmann (LB) scheme for the simulation of droplet formation in microfluidic devices of experimental relevance. The regularized version is shown to provide computationally efficient access to Capillary number regimes relevant to droplet generation via microfluidic devices, such as flow-focusers and the more recent microfluidic step emulsifier devices.

1 Introduction

In the last two decades, microfluidic devices have gained a prominent role in several fields of research, from basic fluid dynamics to material science, biomedicine, as well as industrial applications [1, 2, 3]. In the early 2000s, several pioneering works showed the potential of such devices for generating droplets at the microscale with unprecedented degree of uniformity and rational design, thereby establishing the basis of the lab-on-a-chip concept [4, 5, 6, 7]. Nowadays, many publications show that the microfluidics has surged well beyond the proof-of-concept paradigm, proving the viability of the new approach through substantial contributions to chemistry, biology, medicine, 3d-printing, to name but a few [8, 9, 10, 11, 12]. Due to their ease of fabrication via soft lithography methods [13, 14], microfluidic devices are intensely exploited for the study and manipulation of fluids at the submillimeter length scale. In particular, microfluidic devices have been successfully employed for producing porous scaffolding materials with an accurate control over scaffold specifications, such as pore size, shape, distribution and interconnectivity [15, 16].

In such context, droplet generation units are the main component to produce emulsion templating porous materials by means of microfluidic devices. Several droplet-based microfluidic chips include at least one droplet generation unit within different geometries, alongside with droplet splitting/merging units (e.g., flow focusing, coflow, T-, X-, and Y-junctions). Experiments have driven many of the advances in the field. Nonetheless, many quantities of design interest lie still beyond experimental reach, thereby precluding a complete understanding of the basic physics of droplet generation by experimental means and thus holding back further progress in the operation and optimization of microfluidic devices.

Models and simulations may provide valuable insights into basic microfluidic mechanisms. More specifically, computational studies can help elucidating the nature of optimal flow conditions in terms of geometrical and physico-chemical properties, thus facilitating a rational design of the final product.

Over a decade ago, different numerical methods focused on the breakup mechanisms [17, 18], characterizing droplet formation in terms of the relevant dimensionless parameters [19, 20]. In particular, it was noted that by varying volume flow rates of the dispersed and continuous phases, and therefore changing the Reynolds and

*Electronic address: and.montessori@gmail.com; Corresponding author

Capillary numbers, three distinct regimes of formation of droplets can be identified: *squeezing, dripping and jetting*. All three regimes are consistent with experimental observations [4, 21, 22]. The lattice Boltzmann (LB) method has played a major role in the simulation of droplet formation across a wide variety of microfluidic cross-junctions [20, 23, 24, 25, 26].

The LB method is known to experience stability and efficiency limitations at both low and high viscosities [27]; low viscosities are known to threaten numerical stability, while large ones undermine the very hydrodynamic limit of the LB scheme, due to the onset of strong non-equilibrium effects. The latter are raise a specific concern for the simulation microfluidic configurations.

Different strategies can be employed to mitigate the above constraints: the multirelaxation-time (MRT) method [28], and a regularized version (REG) of the standard single-relaxation-time (SRT) LB scheme [29, 30], also known as Regularized lattice Bhatnagar-Gross-Krook model, as well as the entropic version of the LB method [31].

In this paper, we investigate and demonstrate the benefits of the regularization procedures, as applied to the color gradient model introduced by Leclaire and co-workers [32, 33], for the simulation of microfluidic devices.

Indeed, the REG approach filters out the non-hydrodynamic modes, also known as ghost-modes, originating from non-equilibrium effects stemming from free molecular motion between two subsequent collisions [30, 34, 35, 36].

As detailed in the sequel, this proves particularly useful for microfluidic applications characterised by low Capillary numbers.

The paper is organized as follows. In Sec. II the lattice Boltzmann equation with the BGK collisional operator is described, together with the colour gradient model for simulating multicomponent fluids and the regularization algorithm. In Sec. III the regularization algorithm is commented and its benefits for LB simulation in microfluidics context are highlighted. Section IV presents the results of flow-focusing simulations in two spatial dimensions as well as preliminary three-dimensional simulations of the newly proposed "volcano" micro devices. Finally, a summary is provided in Sec. V.

2 Methods

The LB immiscible multi-component model is based on the following lattice Bhatnagar-Gross-Krook (BGK) equation:

$$f_i^k(\vec{x} + \vec{c}_i \Delta t, t + \Delta t) = f_i^k(\vec{x}, t) + \Omega_i^k(f_i^k(\vec{x}, t)), \quad (1)$$

where f_i^k is the discrete distribution function, representing the probability of finding a particle of the k -th component at position \vec{x} and time t with discrete velocity \vec{c}_i . The lattice time step is taken equal to 1, and i the index spans the lattice discrete directions $i = 0, \dots, b$ [33]. The density ρ^k of the k -th fluid component is given by the zeroth moment of the distribution functions

$$\rho^k(\vec{x}, t) = \sum_i f_i^k(\vec{x}, t), \quad (2)$$

while the total momentum $\rho \vec{u}$ is defined by the first order moment:

$$\rho \vec{u} = \sum_i \sum_k f_i^k(\vec{x}, t) \vec{c}_i. \quad (3)$$

The collision operator Ω_i^k results from the combination of three sub-operators, namely [37, 33]

$$\Omega_i^k = (\Omega_i^k)^{(3)} \left[(\Omega_i^k)^{(1)} + (\Omega_i^k)^{(2)} \right]. \quad (4)$$

Here, $(\Omega_i^k)^{(1)}$ is the standard BGK operator for the k -th component, accounting for relaxation towards a local equilibrium

$$(\Omega_i^k)^{(1)} f_i^k(\vec{x}, t) = f_i^k(\vec{x}, t) - \omega_k \left(f_i^k(\vec{x}, t) - f_i^{k,eq}(\vec{x}, t) \right), \quad (5)$$

where ω_k is the relaxation rate, and $f_i^{k,eq}(\vec{x}, t)$ denotes local equilibria, defined by

$$f_i^{k,eq}(\vec{x}, t) = \rho^k \left[\phi_i^k + w_i \left(\frac{\vec{c}_i \cdot \vec{u}}{c_s^2} + \frac{(\vec{c}_i \cdot \vec{u})^2}{2c_s^4} - \frac{(\vec{u})^2}{2c_s^2} \right) \right]. \quad (6)$$

Here, w_i are weights of the discrete equilibrium distribution functions (e.g. we use a standard D2Q9 lattice), c_s is the lattice sound speed, and ϕ_i^k takes values in D2Q9 lattice

$$\phi_i^k = \begin{cases} \alpha_k, & i = 1, \\ (1 - \alpha_k) / 5, & i = 2, 4, 6, 8, \\ (1 - \alpha_k) / 20, & i = 3, 5, 7, 9, \end{cases} \quad (7)$$

where we number $i = 2, 4, 6, 8$ the nearest-neighbour lattice displacements, and $i = 3, 5, 7, 9$ the diagonal ones. In the above expression, α_k is a free parameter, modulating the density ratio γ_k of the k -th component with respect to the others [38], as well as tuning its relative pressure

$$p^k = \frac{3\rho^k(1 - \alpha_k)}{5}. \quad (8)$$

In this model, $(\Omega_i^k)^{(2)}$ is a perturbation operator, modelling the surface tension of the k -th component. Denoting by \vec{F} the colour gradient in terms of the colour difference, this term reads

$$(\Omega_i^k)^{(2)} f_i^k(\vec{x}, t) = f_i^k(\vec{x}, t) + \frac{A_k}{2} |\vec{F}| \left[w_i \frac{(\vec{F} \cdot \vec{c}_i)^2}{|\vec{F}|^2} - B_i \right], \quad (9)$$

with the free parameters A_k modelling the surface tension, and B_k a parameter depending on the chosen lattice [39, 32].

The above operator models the surface tension, but it does not guarantee the immiscibility between the various components. In order to minimize the mixing of the fluids, a recolouring operator $(\Omega_i^k)^{(3)}$ is introduced. Following the approach in Ref. [32], denoted by ζ and ξ two immiscible fluids, the recolouring operators for the two fluids read as follows"

$$\begin{aligned} (\Omega_i^\zeta)^{(3)} &= \frac{\rho^\zeta}{\rho} f_i + \beta \frac{\rho^\zeta \rho^\xi}{\rho^2} \cos(\phi_i) \sum_k f_i^{k,eq}(\rho^k, 0, \alpha_k) \\ (\Omega_i^\xi)^{(3)} &= \frac{\rho^\xi}{\rho} f_i - \beta \frac{\rho^\zeta \rho^\xi}{\rho^2} \cos(\phi_i) \sum_k f_i^{k,eq}(\rho^k, 0, \alpha_k) \end{aligned} \quad (10)$$

where β is a free parameter and $\cos(\phi_i)$ is the cosine of the angle between the colour gradient \vec{F} and the lattice direction \vec{c}_i . Note that $f_i^{k,eq}(\rho^k, 0, \alpha_k)$ stands for the equilibrium distributions of k -th fluid evaluated using the respective value of ρ^k , zero velocity, and α_k . In the above Eq, $f_i = \sum_k f_i^k$. The LB colour gradient model has been enriched with the so called Regularization procedure [34, 29, 36], namely a discrete Hermite projection of the post-collisional set of distribution functions onto a proper set of Hermite basis. The main idea is to introduce a set of pre-collision distribution functions which are defined only in terms of the macroscopic hydrodynamic moments.

$$f_i^k(x_i + c_i \Delta t, t + \Delta t) = \mathcal{R} f_i^{k,neq}(x, t) \equiv h_i^{k,eq} - \frac{\Delta t}{\tau} h_i^{k,neq} \quad (11)$$

where h_i^k is the hydrodynamic component of the full distribution f_i^k (see [29]) for the k -th colour, and \mathcal{R} is the regularization operator. The above equation shows that the post-collision distribution, of a 4th-order isotropic lattice, is defined only in terms of the conserved and the transport hydrodynamic modes, namely density ρ , current $\rho \vec{u}$ and momentum-flux tensor $\mathbf{\Pi} = \sum_i f_i \vec{c}_i \vec{c}_i$. The motivation for using the regularization procedure in the colour gradient model is detailed in the next Section.

3 Regularized LB multicomponent approach for low Capillary and Reynolds microfluidics

The Reynolds and the Capillary numbers are defined as follows:

$$\begin{aligned} Ca &= \frac{\rho \nu U}{\sigma} \\ Re &= \frac{LU}{\nu} \end{aligned} \quad (12)$$

where ν is the kinematic viscosity of the fluid, σ is the surface tension and L and U are respectively, the characteristic length and velocity. Microfluidic flows in T-junctions and flow focusing devices are most often characterized by $Re \sim 1$ and $Ca \ll 1$. For a typical droplet of diameter $D = 10^{-4}$ (m), moving at a speed $U = 0.01$ (m/s) the Reynolds and Capillary numbers are $Re = 10$ and $Ca = 10^{-4}$, where we have taken the density of water and a surface tension of $\sim 10mN/m$. The diffuse nature of the fluid-fluid interface in the multicomponent model employed in this work, poses some constraint on the ratio between the characteristic length scale of the problem, namely the droplet diameter D , and the width of the diffuse interface, δ , known as Cahn number $Cn = \delta/D$ [40]. Since the interface width lies on nanometric scales, the Cahn number is usually very small, of the order of 10^{-4} or less. Such scale separation is computationally unpractical, and LB simulations must typically operate at much higher Cahn numbers, between $0.01 \div 0.1$, implying that the

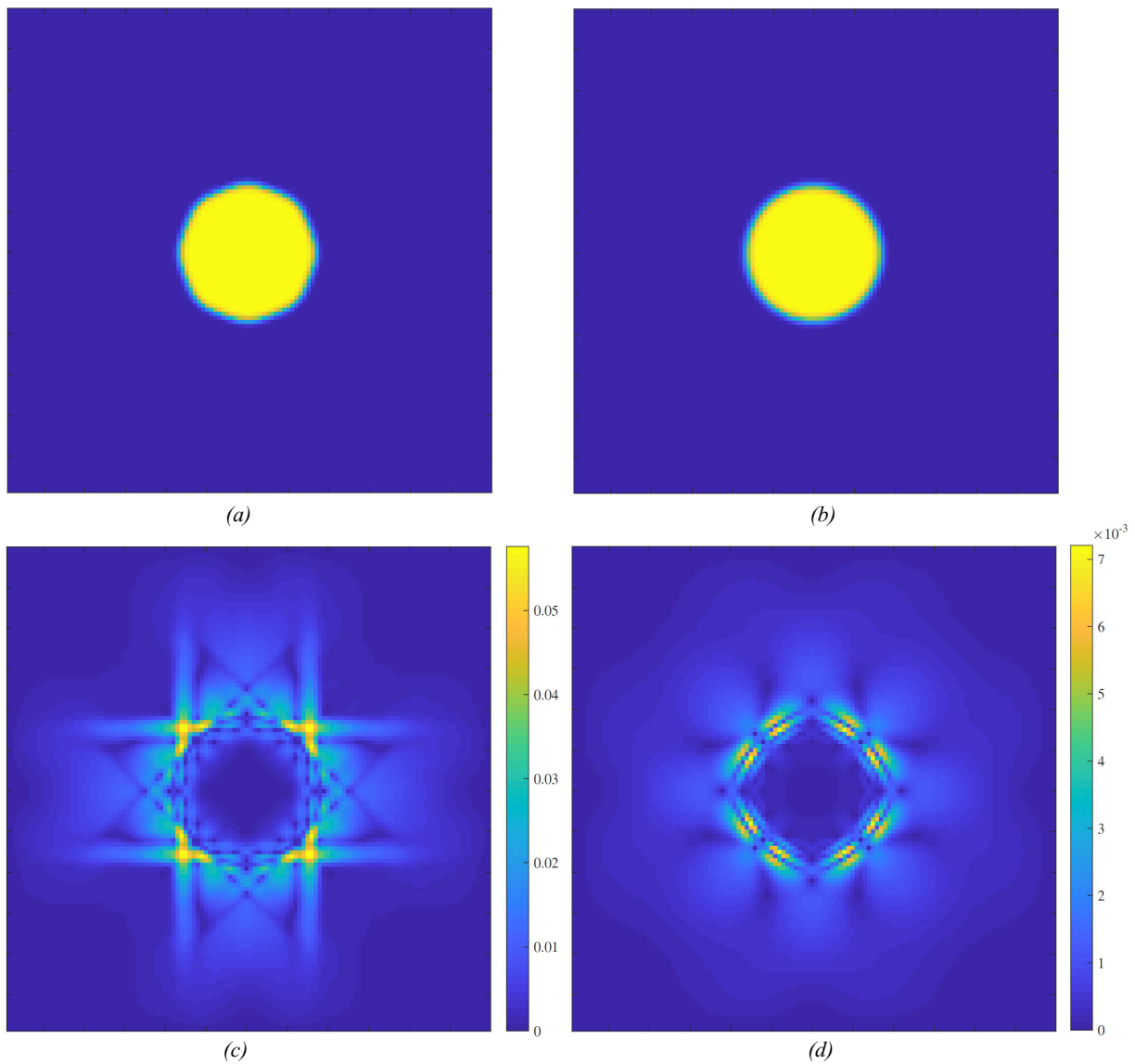


Figure 1: (a) and (b); density field of a resting droplet immersed in a second component : (a) LBGK (b) Regularized LBGK. The relaxation times of the blue and yellow component were set, respectively, to 1 and 5 ($\nu_B \sim 0.167$, $\nu_Y \sim 1.5$). (b) and (c) velocity field (spurious currents) around the resting droplets for the non regularized (b) and Regularized (c) case. It is evident that, for high viscosity values of the dispersed phase, a reduction of isotropy emerges that reflects into a non spherical shape of the resting droplet. An inspection of the flow field highlights that the droplet anisotropy is basically driven by a non-physical flow field around the droplet which is, in turn, caused by the presence of the ghost modes which are excited in the under-relaxed regime ($\tau > 1$). As one can see, the Regularization cures the loss of isotropy in under-relaxed LBGK, by suppressing the non-physical modes, as evidenced by the circular shape of the droplet at rest and by the spurious flow field around the droplet, which is now isotropic and roughly an order of magnitude smaller than in the plain LBGK case.

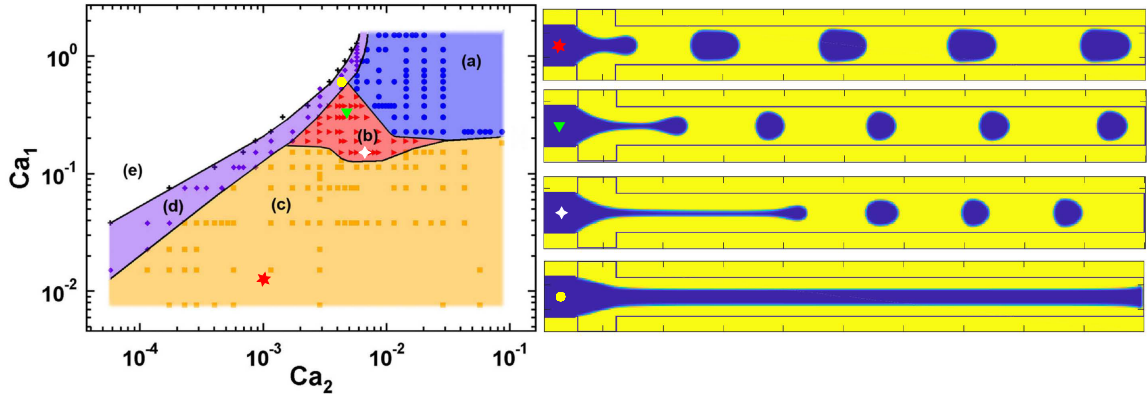


Figure 2: Capillary number-based flow map with flow regimes reproduced by the regularized color gradient model (from the upper left to the lower left panel): Dripping, jetting (second and third) and tubing. The regularized model is capable of accurately predicting the different flow regimes in a microfluidic flow focusing device. The viscosities of the two fluids are $\nu_Y = 0.167$ (continuous phase) and $\nu_B \sim 0.5$ (dispersed phase), thus matching the viscosity ratio of the liquids employed in the experiments reported in [41].

associated inaccuracies must be properly inspected. Given that the diffuse interface is about 5 lattice units, by taking $D_{lb} = 100$ (subscript lb denotes lattice units), we obtain $Cn = 0.05$. Realizing $Re = 1$ with $Cn \sim 0.05$ runs against numerical limitations of the LB method; for instance, by choosing $U_{lb} = 0.001$ and $\nu_{lb} = 0.1$, one faces two inconveniences: first, very long simulation time due to the small velocities, ($U_{lb} = 0.001$ means thousands lattice time steps to cover one lattice spacing...), second, a low signal/noise ratio due to spurious currents. The alternative is to raise both the velocity and the viscosity, say $U_{lb} = 0.01$ and $\nu_{lb} = 1$; however, this implies large values of the relaxation time τ , triggering correspondingly large non-equilibrium effects and ghost currents. This is where the benefits of the Regularization technique take stage: by filtering out the ghost currents, the Regularized LB can operate at higher values of the droplet speed without incurring into spurious currents and anomalous ghost effects, [35].

4 Results

In the following, we present two preliminary applications of the proposed scheme, namely the simulation of droplet formation in standard flow-focussing microfluidic devices and to the recently proposed "volcano" devices [42].

4.1 Flow-focussing devices

We performed simulations of resting droplets of component one (coloured as yellow in Fig. 1) immersed in a second component (blue in Fig. 1) with same densities and different viscosities. The relaxation times of the blue and yellow components were set to 1 and 5 ($\nu_B \sim 0.167$, $\nu_Y \sim 1.5$), respectively. It is worth to highlight that, for high viscosity values of the dispersed phase, sizeable non-isotropic effects arise, resulting in a non-spherical shape of the rest droplet. A more detailed inspection of the flow field shows that the droplet anisotropy is basically driven by a non-physical flow field around the droplet, caused by the presence of the ghost modes. The ghost modes are excited whenever under-relaxed ($\tau > 1$) LBGK models are employed [35]. The regularization cures the loss of isotropy in under-relaxed LBGK, by suppressing the non-physical modes as evidenced by the circular shape of the droplet at rest and by the spurious flow field around the droplet (see Fig. 1 left panels) which is isotropic. Further, the maximum value of spurious currents is an order of magnitude smaller than in the plain LBGK case. We then run simulations of a flow focusing device and compared our results with experimental data available in literature. The viscosities of the two fluids are $\nu_Y = 0.167$ (continuous phase) and $\nu_B \sim 0.5$ (dispersed phase), thus matching the viscosity ratio of the liquids employed in the experiments of Ref. [41]. Even in this case, the relaxation time of the dispersed phase (blue in Fig. 2) is greater than one, providing an out of equilibrium regime as in the previous case. In Fig. 2 we report the Capillary number-based flow map with flow regimes by Cubaud et al. [41]. The regularized colour gradient is clearly able to reproduce the different flow regimes in such microfluidic flow-focussing device, correctly predicting dripping, jetting and tubing flow configurations at different Capillary numbers. Next, we computed the normalized droplet diameter d/h , being h the height of the microfluidic channel, versus the flow rate ratio (Q_B/Q_Y) and compare with experimental data. The numerical results, in agreement with Ref. [41], collapse on a single master curve, which scales with the flow rate like $Q_B/(2Q_Y)^{0.5}$ (see Fig. 3). As a prospective application, the regularized approach

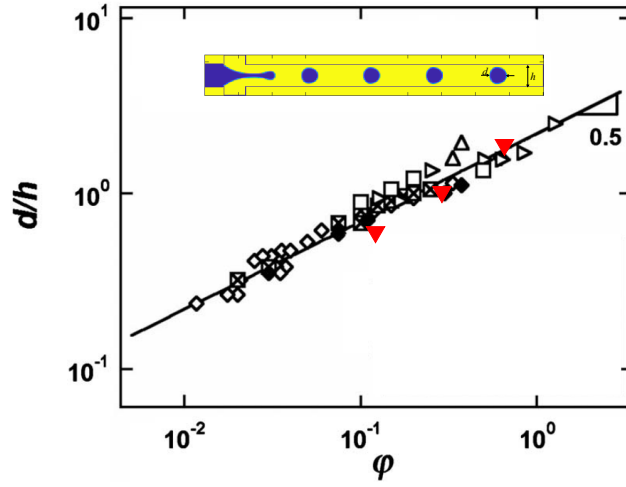


Figure 3: Normalized droplet diameter d/h vs the flow rate ratio $\phi = Q_B/Q_Y$. Numerical results (Red triangles) are superimposed to the experimental curve of Cubaud et al. [41]. The diameters collapse on a single master curve, which scales with the flow rate like $Q_B/(2Q_Y)^{0.5}$, as reported in [41].

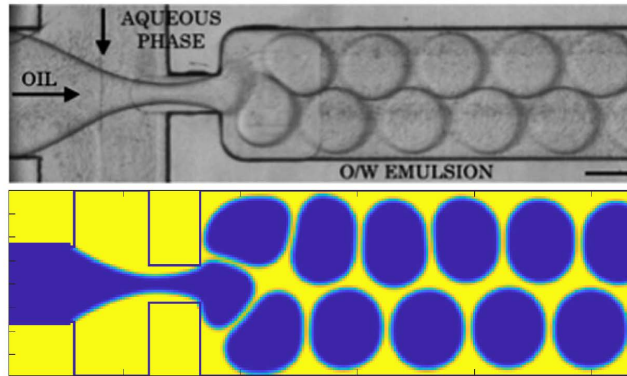


Figure 4: Prospective application of regularized colour gradient model augmented with arrested coalescence algorithm. The model allows for stable simulation of mono-disperse droplets. This opens the way to the simulation of mono-dispersed oil-water emulsions. Future applications of this model will allow to identify optimal operational regimes, capable of delivering droplet configurations of high regularity, both in size and connectivity. Upper panel containing the experimental data is reported from Ref. [15]

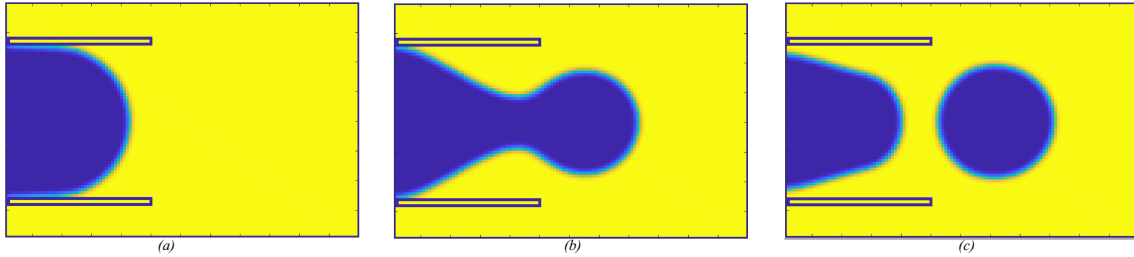


Figure 5: Density field at the $x - z$ Mid-plane of the nozzle of the volcano device. The width of the channel $w = 700\mu\text{m}$ and the height $h = 70\mu\text{m}$ ($h/w = 1/10$), corresponding to Capillary number is $Ca = 1.4 \times 10^{-2}$. After the break up, the droplet diameter is $D = 350\mu\text{m}$, so that $D/w = 0.5$, in good agreement with the experimental findings on the volcano device ($w/h = 8$, $D/w = 0.58$, $Ca = 10^{-2}$) [42].

was used to simulate an oil/water emulsion in a flow-focusing device. In order to obtain a mono-dispersed emulsion, the regularized colour gradient approach has been augmented with an algorithm aimed at suppressing coalescence between the droplets of the dispersed phase (oil). The results show that the model allows for stable simulation of mono-disperse droplets, well reproducing the experimental data (see upper panel of Fig. 4). This opens the way to the simulation of mono-dispersed oil-water emulsions. Future applications of this model will allow to identify optimal operational regimes capable of delivering droplet configurations of high regularity, both in size and connectivity.

4.2 Microfluidic volcanos

As a further application, we report some preliminary simulations of a new class of step emulsification devices, called volcano [42], which are based on the idea of preventing the obstruction of the nozzles from the droplets via buoyancy effects. These devices are expected to enhance the yield of highly mono-dispersed water/oil emulsion, which is highly desirable for most industrial purposes.

The volcano device made from polydimethylsiloxane is used here for producing water in oil emulsions. The water flows through the device inlet, and splits into hundreds of step-emulsifier nozzles with rectangular cross section. The device is submerged in a quiescent oil reservoir, each nozzle producing a stream of micron-sized droplets.

As a preliminary step, we simulated a single-nozzle device. Upon matching the governing dimensionless groups (Capillary and Weber number) and the characteristic geometrical ratio h/w (see the caption of fig. 5 for the values of the physical parameters), we are able to simulate the droplet break up. After the break up, the droplet diameter is $D \sim 350\mu\text{m}$, corresponding to $D/w \sim 0.5$, in good agreement with the experimental findings on the volcano device ([42]) ($w/h = 8$, $D/w = 0.58$, $Ca = 10^{-2}$). A thorough investigation of the microfluidics of volcano devices is currently underway, and will make the subject of future communications.

5 Summary

Summarising, we have presented a novel variant of the Lattice Boltzmann method for multiphase flows, based on the regularisation of the colour-gradient scheme, augmented with a color-swap algorithm to mimic the effect of intermolecular repulsion, so as to tame droplet coalescence. The new scheme has been applied to the simulation of droplet production in flow-focussing micro-devices, finding satisfactory agreement with the existing literature, both in terms of predicting the transition from dripping-jetting-tubing regimes, and also in terms of spacetime patterns of the droplet configurations in experimental devices. Moreover, we have also presented preliminary three-dimensional simulations of an alternative step emulsifier device, known as volcano device, which is based on the idea of promoting nozzles cleaning via buoyancy effects. If successfully demonstrated, volcano devices may offer substantial advantages in terms of droplet rate production, degree of mono-dispersity and morphological regularity.

Acknowledgments

The research leading to these results has received funding from the European Research Council under the European Union's Horizon 2020 Framework Programme (No. FP/2014- 2020)/ERC Grant Agreement No. 739964 ("COPMAT").

References

- [1] S. L. Anna, Droplets and bubbles in microfluidic devices, *Annual Review of Fluid Mechanics* 48 (2016) 285–309.
- [2] G. T. Vladislavljević, N. Khalid, M. A. Neves, T. Kuroiwa, M. Nakajima, K. Uemura, S. Ichikawa, I. Kobayashi, Industrial lab-on-a-chip: Design, applications and scale-up for drug discovery and delivery, *Advanced drug delivery reviews* 65 (11) (2013) 1626–1663.
- [3] A. B. Theberge, F. Courtois, Y. Schaerli, M. Fischlechner, C. Abell, F. Hollfelder, W. T. Huck, Microdroplets in microfluidics: an evolving platform for discoveries in chemistry and biology, *Angewandte Chemie International Edition* 49 (34) (2010) 5846–5868.
- [4] A. Utada, E. Lorenceau, D. Link, P. Kaplan, H. Stone, D. Weitz, Monodisperse double emulsions generated from a microcapillary device, *Science* 308 (5721) (2005) 537–541.
- [5] S. L. Anna, N. Bontoux, H. A. Stone, Formation of dispersions using "flow focusing" in microchannels, *Applied physics letters* 82 (3) (2003) 364–366.
- [6] A. M. Gañán-Calvo, J. M. Gordillo, Perfectly monodisperse microbubbling by capillary flow focusing, *Physical review letters* 87 (27) (2001) 274501.
- [7] T. Thorsen, R. W. Roberts, F. H. Arnold, S. R. Quake, Dynamic pattern formation in a vesicle-generating microfluidic device, *Physical review letters* 86 (18) (2001) 4163.
- [8] E. K. Sackmann, A. L. Fulton, D. J. Beebe, The present and future role of microfluidics in biomedical research, *Nature* 507 (7491) (2014) 181.
- [9] J. Rodríguez-Rodríguez, A. Sevilla, C. Martínez-Bazán, J. M. Gordillo, Generation of microbubbles with applications to industry and medicine, *Annual Review of Fluid Mechanics* 47 (2015) 405–429.
- [10] K. S. Elvira, X. C. i Solvas, R. C. Wootton, et al., The past, present and potential for microfluidic reactor technology in chemical synthesis, *Nature chemistry* 5 (11) (2013) 905–915.
- [11] L. Mazutis, J. Gilbert, W. L. Ung, D. A. Weitz, A. D. Griffiths, J. A. Heyman, Single-cell analysis and sorting using droplet-based microfluidics, *Nature Protocols* 8 (5) (2013) 870–891.
- [12] N. Bhattacharjee, A. Urrios, S. Kang, A. Folch, The upcoming 3d-printing revolution in microfluidics, *Lab on a Chip* 16 (10) (2016) 1720–1742.
- [13] J. McDonald, D. Duffy, J. Anderson, D. Chiu, H. Wu, O. Schueller, G. Whitesides, Fabrication of microfluidic systems in poly (dimethylsiloxane)., *Electrophoresis* 21 (1) (2000) 27–40.
- [14] G. M. Whitesides, A. D. Stroock, Flexible methods for microfluidics, *Phys. Today* 54 (6) (2001) 42–48.
- [15] M. Costantini, C. Colosi, J. Guzowski, A. Barbetta, J. Jaroszewicz, W. Świążkowski, M. Dentini, P. Garstecki, Highly ordered and tunable polyhypes by using microfluidics, *Journal of Materials Chemistry B* 2 (16) (2014) 2290–2300.
- [16] B. H. Oh, A. Bismarck, M. B. Chan-Park, Injectable, interconnected, high-porosity macroporous biocompatible gelatin scaffolds made by surfactant-free emulsion templating, *Macromolecular rapid communications* 36 (4) (2015) 364–372.
- [17] M. M. Dupin, I. Halliday, C. M. Care, Simulation of a microfluidic flow-focusing device, *Physical review E* 73 (5) (2006) 055701.
- [18] M. De Menech, Modeling of droplet breakup in a microfluidic t-shaped junction with a phase-field model, *Physical Review E* 73 (3) (2006) 031505.
- [19] M. De Menech, P. Garstecki, F. Jousse, H. Stone, Transition from squeezing to dripping in a microfluidic t-shaped junction, *journal of fluid mechanics* 595 (2008) 141–161.
- [20] H. Liu, Y. Zhang, Droplet formation in microfluidic cross-junctions, *Physics of Fluids* 23 (8) (2011) 082101.
- [21] P. Garstecki, M. J. Fuerstman, H. A. Stone, G. M. Whitesides, Formation of droplets and bubbles in a microfluidic t-junction-scaling and mechanism of break-up, *Lab on a Chip* 6 (3) (2006) 437–446.
- [22] A. S. Utada, A. Fernandez-Nieves, H. A. Stone, D. A. Weitz, Dripping to jetting transitions in coflowing liquid streams, *Physical review letters* 99 (9) (2007) 094502.

- [23] W. Wang, Z. Liu, Y. Jin, Y. Cheng, Lbm simulation of droplet formation in micro-channels, *Chemical engineering journal* 173 (3) (2011) 828–836.
- [24] G. Falcucci, S. Ubertini, D. Chiappini, S. Succi, Modern lattice boltzmann methods for multiphase microflows, *IMA journal of applied mathematics* 76 (5) (2011) 712–725.
- [25] Y. Yan, D. Guo, S. Wen, Numerical simulation of junction point pressure during droplet formation in a microfluidic t-junction, *Chemical engineering science* 84 (2012) 591–601.
- [26] A. Gupta, M. Sbragaglia, A lattice boltzmann study of the effects of viscoelasticity on droplet formation in microfluidic cross-junctions, *The European Physical Journal E* 39 (1) (2016) 2.
- [27] C. K. Aidun, J. R. Clausen, Lattice-boltzmann method for complex flows, *Annual review of fluid mechanics* 42 (2010) 439–472.
- [28] F. Higuera, S. Succi, R. Benzi, Lattice gas dynamics with enhanced collisions, *EPL (Europhysics Letters)* 9 (4) (1989) 345.
- [29] R. Zhang, X. Shan, H. Chen, Efficient kinetic method for fluid simulation beyond the navier-stokes equation, *Physical Review E* 74 (4) (2006) 046703.
- [30] J. Latt, B. Chopard, Lattice boltzmann method with regularized pre-collision distribution functions, *Mathematics and Computers in Simulation* 72 (2) (2006) 165–168.
- [31] S. Ansumali, I. Karlin, C. E. Frouzakis, K. Boulouchos, Entropic lattice boltzmann method for microflows, *Physica A: Statistical Mechanics and its Applications* 359 (2006) 289–305.
- [32] S. Leclaire, M. Reggio, J.-Y. Trépanier, Isotropic color gradient for simulating very high-density ratios with a two-phase flow lattice boltzmann model, *Computers & Fluids* 48 (1) (2011) 98–112.
- [33] S. Leclaire, M. Reggio, J.-Y. Trépanier, Numerical evaluation of two recoloring operators for an immiscible two-phase flow lattice boltzmann model, *Applied Mathematical Modelling* 36 (5) (2012) 2237–2252.
- [34] A. Montessori, G. Falcucci, P. Prestininzi, M. La Rocca, S. Succi, Regularized lattice bhatnagar-gross-krook model for two-and three-dimensional cavity flow simulations, *Physical Review E* 89 (5) (2014) 053317.
- [35] A. Montessori, P. Prestininzi, M. La Rocca, S. Succi, Lattice boltzmann approach for complex nonequilibrium flows, *Physical Review E* 92 (4) (2015) 043308.
- [36] G. Falcucci, A. Montessori, S. Succi, On the effects of reactant flow rarefaction on heterogeneous catalysis: a regularized lattice boltzmann study, *Communications in Computational Physics* doi:10.4208/cicp.0A-2016-0250.
- [37] J. Tölke, Lattice boltzmann simulations of binary fluid flow through porous media, *Philosophical Transactions of the Royal Society of London A: Mathematical, Physical and Engineering Sciences* 360 (1792) (2002) 535–545.
- [38] D. Grunau, S. Chen, K. Eggert, A lattice boltzmann model for multiphase fluid flows, *Physics of Fluids A: Fluid Dynamics* 5 (10) (1993) 2557–2562.
- [39] T. Reis, T. Phillips, Lattice boltzmann model for simulating immiscible two-phase flows, *Journal of Physics A: Mathematical and Theoretical* 40 (14) (2007) 4033.
- [40] J. W. Cahn, J. E. Hilliard, Free energy of a nonuniform system. i. interfacial free energy, *The Journal of chemical physics* 28 (2) (1958) 258–267.
- [41] T. Cubaud, T. G. Mason, Capillary threads and viscous droplets in square microchannels, *Physics of Fluids* 20 (5) (2008) 053302.
- [42] E. Stolovicki, R. Ziblat, D. A. Weitz, Throughput enhancement of parallel step emulsifier devices by shear-free and efficient nozzle clearance, submitted to *Lab on a Chip*.